



Correlation of autopsy pathological findings and imaging features from 9 fatal cases of COVID-19 pneumonia

Lingyun Zhao, MD^a, Xi Wang, MD^b, Ying Xiong, MD^{a,*} , Yanqing Fan, MD^c, Yiwu Zhou, PhD^d, Wenzhen Zhu, PhD^a 

Abstract

We aimed to investigate the relationship of radiological features and the corresponding pulmonary pathology of patients with Coronavirus Disease (COVID-19) pneumonia.

In this multicenter study, serial chest CT and radiographic images from 9 patients (51–85 years old, 56% male) were reviewed and analyzed. Postmortem lungs were sampled and studied from these autopsies, with a special focus on several corresponding sites based on imaging features.

The predominant pattern of pulmonary injury in these 9 cases was diffuse alveolar damage (DAD) and interstitial inflammation. Moreover, acute fibrinous exudates, organization, inflammatory cell infiltration, hyaline membranes, pulmonary edema, pneumocyte hyperplasia, and fibrosis were all observed. The histopathology features varied according to the site and severity of each lesion. In most of the 9 cases, opacities started from a subpleural area and peripheral structures were more severely damaged based on gross views and pathological examinations. Fibrosis could occur in early stages of infection and this was supported by radiological and pathological findings. The radiological features of COVID-19 pneumonia, at the critically ill stage, were diffuse ground-glass opacities with consolidation, interstitial thickening, and fibrous stripes, which was based in the fibrous tissue proliferation in the alveolar and interlobular septa, and filled alveoli with organizing exudation. Fungal and bacterial co-infections were also observed in 6 cases.

Typical imaging features can be correlated with underlying pathological findings. Combining assessments of imaging features with pathological findings therefore can enhance our understanding of the histopathological mechanism of COVID-19 pneumonia, and facilitate early radiological diagnosis and prognosis estimation of COVID-19 pneumonia, which has important implications for the development of clinical targeted treatments and research related to COVID-19 pneumonia.

Abbreviations: COVID-19 = Coronavirus Disease 2019, CR = chest radiography, CT = computed tomography, DAD = diffuse alveolar damage, GGO = ground-glass opacities.

Keywords: co-infections, Coronavirus Disease 2019 pneumonia, fibrosis, radiological and pathological features

Editor: Nesreen E. Morsy.

LZ and XW contributed equally.

This work was supported by the National Natural Science Foundation of China (grant number 81730049).

The authors have no conflicts of interests to disclose.

The datasets generated during and/or analyzed during the current study are available from the corresponding author on reasonable request.

^aDepartment of Radiology, ^bDepartment of Pathology, Tongji Hospital, Tongji Medical College, Huazhong University of Science and Technology, ^cDepartment of Radiology, Jin Yin-tan Hospital, ^dDepartment of Forensic Medicine, Tongji Medical College, Huazhong University of Science and Technology, Wuhan, China.

* Correspondence: Ying Xiong, Department of Radiology, Tongji Hospital, Tongji Medical College, Huazhong University of Science and Technology, 1095 Jiefang Ave, Wuhan 430030, China (e-mail: bear1119xy@126.com).

Copyright © 2021 the Author(s). Published by Wolters Kluwer Health, Inc. This is an open access article distributed under the terms of the Creative Commons Attribution-Non Commercial License 4.0 (CCBY-NC), where it is permissible to download, share, remix, transform, and buildup the work provided it is properly cited. The work cannot be used commercially without permission from the journal.

How to cite this article: Zhao L, Wang X, Xiong Y, Fan Y, Zhou Y, Zhu W. Correlation of autopsy pathological findings and imaging features from 9 fatal cases of COVID-19 pneumonia. *Medicine* 2021;100:12(e25232).

Received: 18 September 2020 / Received in final form: 16 January 2021 / Accepted: 26 February 2021

<http://dx.doi.org/10.1097/MD.00000000000025232>

1. Introduction

Coronavirus Disease 2019 (COVID-19) is a highly infectious disease associated with SARS-CoV-2, which is highly homologous to SARS-CoV, a virus that belongs to the family Coronaviridae.^[1,2] Cases from more than 200 countries and regions have been reported. Among all confirmed cases, the outbreak of COVID-19 has resulted in 4600 deaths in China and 1,700,000 deaths globally by the end of 2020.^[3]

Abundant previous studies have described the general epidemiological findings, imaging features, clinical course and prognosis of COVID-19 pneumonia.^[4–9] However, complete pathological evidence provided by systematic autopsy is still relatively rare. Radiological examinations are quite readily valuable for diagnosis and reexamination during the course of COVID-19 infection. The typical radiological features of COVID-19 pneumonia include ground-glass opacities (GGO) with consolidation, interstitial thickening, and fibrous stripes, which usually start from the periphery.^[8–10] Clarifying the underlying pathological evidence of typical imaging features can allow evaluation of the pathogenesis and organ damage of this disease more accurately, which is also conducive to effective clinical treatment and related research.

Here we report the clinical autopsy pathology of COVID-19 pneumonia in 9 patients who died in the Wuhan outbreak. The disease duration was from 14 to 34 days after the onset of

symptoms. For every patient, chest computed tomography (CT) and chest radiography (CR) were of great importance and were applied several times in reexaminations of disease progression. Final CT and CR findings were retrospectively investigated and compared with corresponding pathological changes in order to explore the pathological evidence of some imaging features and enhance our understanding of both radiological changes and the pathological mechanism of COVID-19 pneumonia. To date, a combination study using radiology and histology in multiple cases has not been emphasized in research on COVID-19 pneumonia.

2. Materials and methods

2.1. Patients

This study was approved by the institutional review board of Tongji Medical College of Huazhong University of Science and Technology and relevant departments (TJ-C20200160). Written informed consent was sought from the patients' families to use their data for research purposes. Postmortem examinations were performed between February 16 and March 2, 2020 on 13 consecutive autopsy patients who died of COVID-19 pneumonia. Their diagnosis of COVID-19 was confirmed with clinical manifestations and positive results to real-time fluorescence polymerase chain reaction (PCR) assay for SARS-CoV-2 nucleic acid. We collected the complete history from symptom onset to all rescue measures to death, including CT and CR data, from 9 of the 13 patients in this study.

2.2. Autopsy and histology

The patients died at several facilities within the Wuhan metropolitan area, and autopsies were conducted in a negative pressure operating room in Wuhan Jin Yin-tan Hospital. Postmortem examinations were conducted by pathologists at the Tongji Medical College of the Huazhong University of Science and Technology in Wuhan, China. All autopsies were done within 24 hours of the patients' death. The highest level of biological safety protections were conducted. The operation, transportation, and preservation of biological test materials conformed to the provisions on autopsy and examination of patients with infectious diseases or suspected infectious diseases (Order No. 43 of the Ministry of Health), the regulations of the National Health Commission of China and the Helsinki Declaration. Hematoxylin

and eosin (HE)-stained slides of lung tissue were reviewed for each patient (ranging from 17 – 50 slides per patient) for multiple histological features. HE-staining findings and their corresponding imaging features were analyzed in detail.

3. Results

3.1. Patient characteristics

Patient characteristics are summarized in Table 1. All patients tested positive for SARS-CoV-2 by nucleic acid test from postmortem lung tissue. The mean age of the group was 69 years (range 51–86 years, median 67 years), and the mean duration of illness from onset of symptoms to death was 25 days (range 14–34 days, median 27 days).

The most common complaints of the patients at onset were fever (6/9 cases), cough (5/9 cases), dyspnea (3/9 cases), fatigue (3/9 cases), chest tightness (2/9 cases), headache (2/9 cases), nausea (1/9 cases) and sore throat (1/9 cases). Abnormalities in blood routine and biochemistry tests were listed in Table 2. Patients received oxygen therapy (up to 15L/minute through face masks and up to 50L/minute through nasal catheters, 9/9 cases), mechanical ventilation (9/9 cases), antiviral agents (acyclovir or ganciclovir, 9/9 cases), antibacterial agents (cephalosporin antibiotics, 7/9 cases), corticosteroids (8/9 cases), and immunoglobulin (6/9 cases). Most of the patients had multiple organ dysfunctions in later stage. Most of the patients developed acute respiratory distress syndrome (ARDS), requiring ICU admission, and unfortunately died from respiratory-circulatory failure. One patient had cardiopulmonary arrest.

3.2. Imaging data

As the course of the disease continued and the patients' conditions deteriorated, radiological examinations showed different characteristics. In the first 14 days of the disease, most patients exhibited progressively more patchy GGO, which started from the subpleural area. Consolidation (5/9 cases), interstitial thickening or reticulation (6/9 cases), fibrous stripes (4/9 cases), and pleural effusion (3/9 cases) were also observed. From 15 to 28 days, more opacities with larger sizes and higher densities were seen bilaterally. More cases with consolidation (6/7 cases), interstitial thickening or reticulation (6/7 cases) were observed [1 patient died at the 14th day and another patient, who died at the

Table 1
Demographics and clinical characteristics of the COVID-19 patients.

Serial number	Gender / Age	Days from onset to death	Days from onset to last CT	Days from onset to last Chest Radiograph	Medical past histories	Comorbidities	Mechanical ventilation
1 (Case1 Fig. 1)	F/66	14	5	9	Hypertension	K, C	Non-invasive
2 (Case2 Fig. 2)	M/85	18	11	-	Hypertension, cerebral infarction	K, C, M, A	Non-invasive
3	F/67	20	10	15	None	L, C, M	invasive
4	F/86	23	7	19	Hypertension, CHD, cerebral infarction	K, C, M, L, A	Non-invasive
5 (Case3 Fig. 3)	M/70	27	12	22	Hypertension	cardiopulmonary arrest	Non-invasive
6	M/78	27	6	25	Hypertension, CHD, T2DM	K, C, M	invasive
7	M/51	29	5	23	Hypertension, Gout	A, C	Non-invasive
8 (Case4 Fig. 4)	M/62	31	24	20	None	K, C	invasive
9 (Case5 Fig. 5)	F/53	34	18	28	None	A, L, C, M	Non-invasive

A = anemia (hemoglobin < 100 g/L and red blood cell count < $3.8 \times 10^{12}/L$), C = coagulation disorders (prothrombin time > 14 seconds, partially activated prothrombin time > 38 seconds and D-dimer > 0.5 $\mu\text{g}/\text{ml}$), CHD = coronary heart disease, K = chronic kidney disease, stage III-V (eGFR < 60 ml/minute/1.73m²), L = liver function damage (alanine aminotransferase > 50 U/L, glutamic oxaloacetic transaminase > 40 U/L and cholinesterase < 4500 U/L), M = myocardial damage (myoglobin > 100 ng/ml, troponin > 0.2 pg/ml and lactate dehydrogenase > 240 U/L), T2DM = type 2 diabetes mellitus.

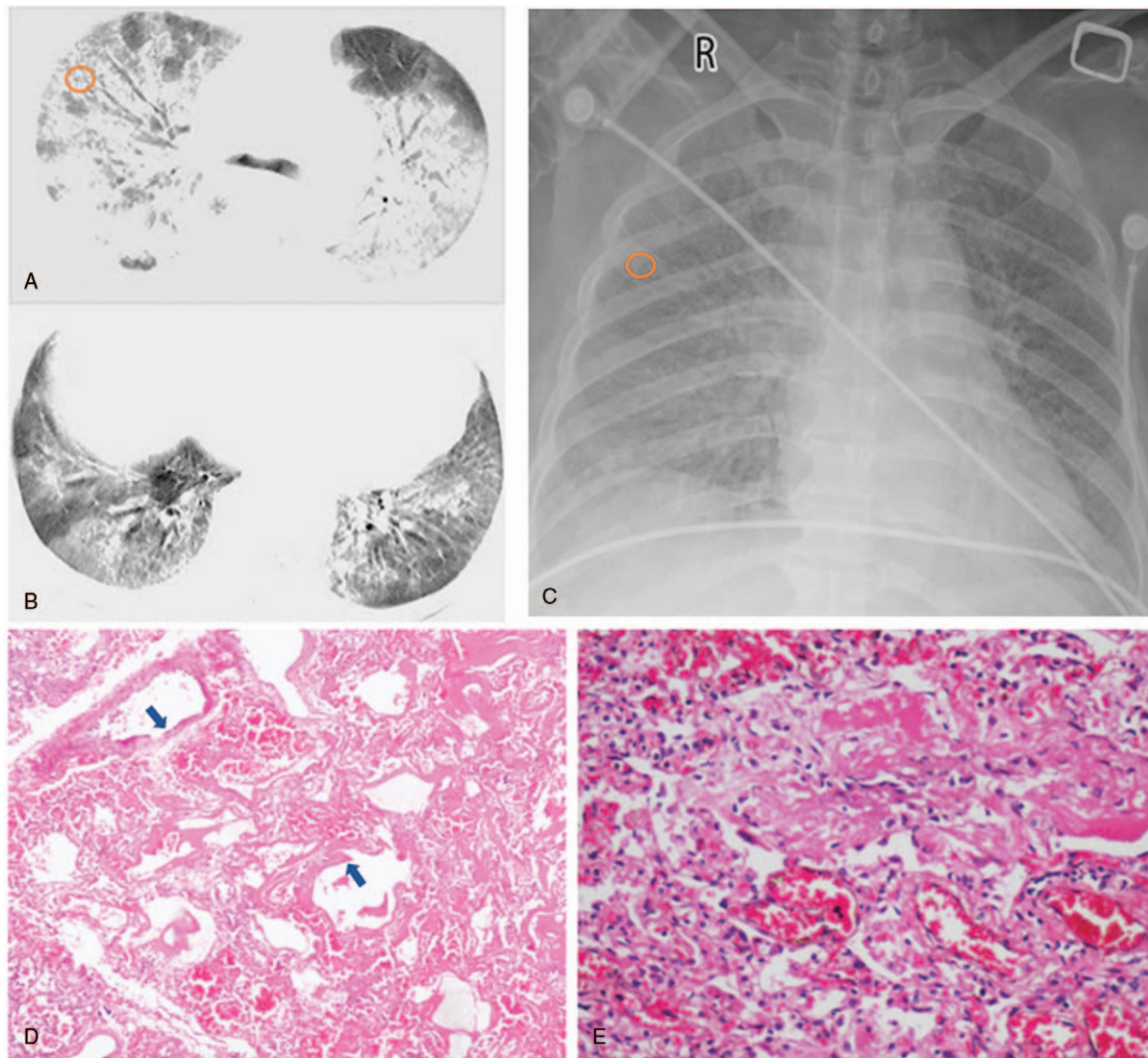


Figure 1. A-B: Large-scale patchy ground-glass opacities with consolidation and interstitial thickening was observed (the 5th day from onset), presenting as “white lungs” in radiographic images. C: The 10th day from onset. D: Exudative phase of diffuse alveolar damage showing hyaline membrane formation (arrows), serous and fibrinous exudate, pulmonary congestion and edema, and small amounts of inflammatory cell infiltration in the right upper lobe ($\times 100$). E: Pulmonary congestion, hemorrhaging, exudate organization in alveolar spaces, and fibrosis of the alveolar septa. Thickened alveolar walls and widened interstitial tissues were accompanied by lymphocytes and other inflammatory cell infiltration and fibroblast proliferation in the right upper lobe ($\times 100$). Yellow circles in figures represent pathological sampling sites.

18th day, did not take radiological exams in this period (15–28 days)]. Two patients survived after 28 days and one of them took the final CR exam at this stage, which showed multiple and large-scale patchy GGOs and consolidation, as well as interstitial thickening or reticulation. In most cases (8/9 cases), their last CT or CR images (usually bedside chest films) exhibited diffuse bilateral lesions, which presents as “white lungs”.

3.3. Pathological findings

At a gross level view, the lungs appeared congested and showed areas of consolidation, harder than is normally observed. Pulmonary necrosis also occurred. Some of the pulmonary lobules were filled and whitened, mixed with dark-red congestion and hemorrhaging. Lesions in the margin areas were more severe than other locations. The basic pathological features included localized or diffuse alveolitis and interstitial inflammation. The

histologic findings also exhibited some unique characteristics. First, serous, fibrinous exudate, and hyaline membrane formations were observed in alveolar spaces. The exudate cells were mainly composed of monocytes and macrophages. Multinucleated giant cells were also seen. Second, there were hyperemia, edema, infiltration of monocytes and lymphocytes within the septa, and thrombus in the pulmonary arteries. Third, pulmonary interstitial fibrosis, type II alveolar epithelium proliferation and organized exudate in alveoli were observed. Fourth, exfoliated epithelium of the bronchial mucosa, occasionally with mucus plugs, were seen in the lumen. These changes were consistent with diffuse alveolar damage (DAD) and presented bilaterally. Secondary infections (bacterial or fungal infections) were seen in 6/9 cases. The pulmonary histologic features of the 9 COVID-19 cases are summarized in Table 3. All patients showed predominantly a DAD pattern of lung injury, with formation of hyaline membranes and interstitial fibrous tissue proliferation.

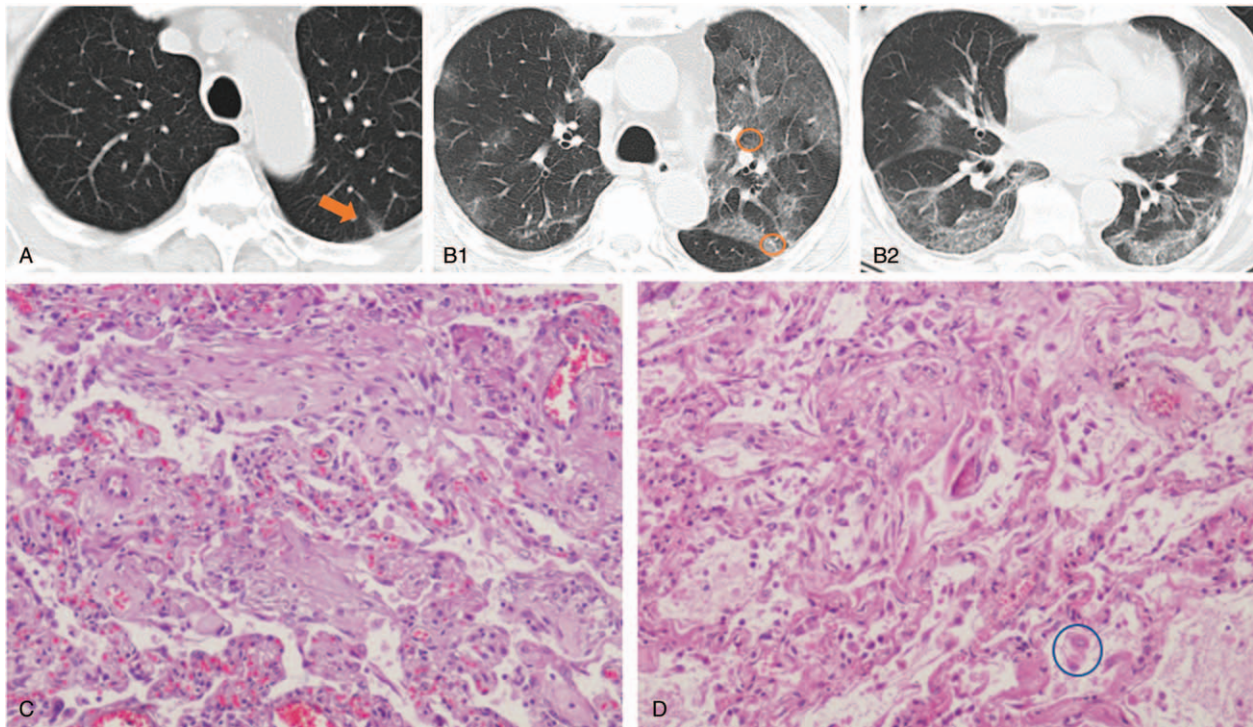


Figure 2. A: In early stage of the disease, a very small ground-glass opacity originated from the subpleural area (arrow, the 3rd day from onset). B1: Several days later, multiple opacities were observed bilaterally, especially in the left upper lobe, combined with the “paving stone signs” (the 12th day from onset). B2: Ground-glass opacities with interlobular septal thickening and fibrosis stripes. C: In the subpleural portion of the left upper lobe, fibrous tissue proliferation in the alveolar septa, alveolar collapse, alveolar epithelium exfoliation and adenoid alveolar formation ($\times 100$). D: In the central part of the left upper lobe, the alveolar structure was roughly preserved, small foci fibrosis of alveolar septa with widened alveolar walls, type II pneumocytes hyperplasia, and serous, lymphocytes, monocytes and macrophage exudation (blue circle) in the alveolar spaces ($\times 100$). Yellow circles: subpleural and central pathological sampling sites.

Five of the 9 cases: 2 patients with shorter course (14 and 18 days), 1 patient with a median course of the disease (27 days), and 2 patients with a longer course of the disease (31 and 34 days), were reported as representatives below.

3.4. Case 1 (Fig. 1)

A 66 year old female patient, whose disease duration from onset of symptoms to death was 14 days. She complained of low fever (38°C), asthenia and chest tightness for 2 days before admitted in hospital. At admission, the lymphocyte count was 9.7%, CRP was 126.3 mg/L, and ESR was 26 mm/hour.

3.5. Case 2 (Fig. 2)

An 85 year old male patient who was admitted to the hospital because of cerebral infarction. During hospitalization, he complained of emerging cough and throat pain. He was diagnosed with COVID-19 pneumonia later. The total disease duration from onset of respiratory symptoms (cough and throat pain) to death was 18 days.

3.6. Case 3 (Fig. 3)

A 70 year old male patient whose disease duration was 27 days. Fatigue, headache and anorexia occurred after he caught cold. The symptoms quickly got worse. He felt short of breath particularly after activities. At admission, the body temperature was 38°C , WBC was $2.6 \times 10^9/\text{L}$, lymphocyte count was $0.61 \times 10^9/\text{L}$, and CRP was 225.8 mg/L.

3.7. Case 4 (Fig. 4)

A 62 year old male patient whose disease duration was 27 days. He complained of intermittent low fever and dry cough for 16 days. His disease duration from onset of symptoms to death was 31 days. At admission, the lymphocyte count was 6.5%, CRP was 160.0 mg/L and ESR was 44 mm/hour.

3.8. Case 5 (Fig. 5)

A 53 year old female patient whose disease duration was 34 days. During the whole course of treatment, chest radiographic images showed that the lung lesions had improved for a time (around the 26th day of infection, Fig. 5B). After that, however, persistent deterioration of lung function, manifested by dyspnea and reduced oxygen saturation, was observed. Meanwhile, WBC counts and neutrophil ratios increased continuously, from $9.5 \times 10^9/\text{L}$ to $16.5 \times 10^9/\text{L}$ and 93% to 96%, respectively. A combination of bacterial infections in later stages of infection were highly suspected.

4. Discussion

The predominant patterns of pulmonary injury in the 9 cases were DAD and interstitial inflammation. At the onset of the disease, the early CT manifestations of COVID-19 pneumonia were typical, with most GGO lesions distributed in the posterior area and pulmonary periphery.^[8–10] The key receptor of SARS-CoV-2, the angiotensin converting enzyme 2 (ACE2), is highly expressed in pulmonary capillary endothelial cells, the epithelium

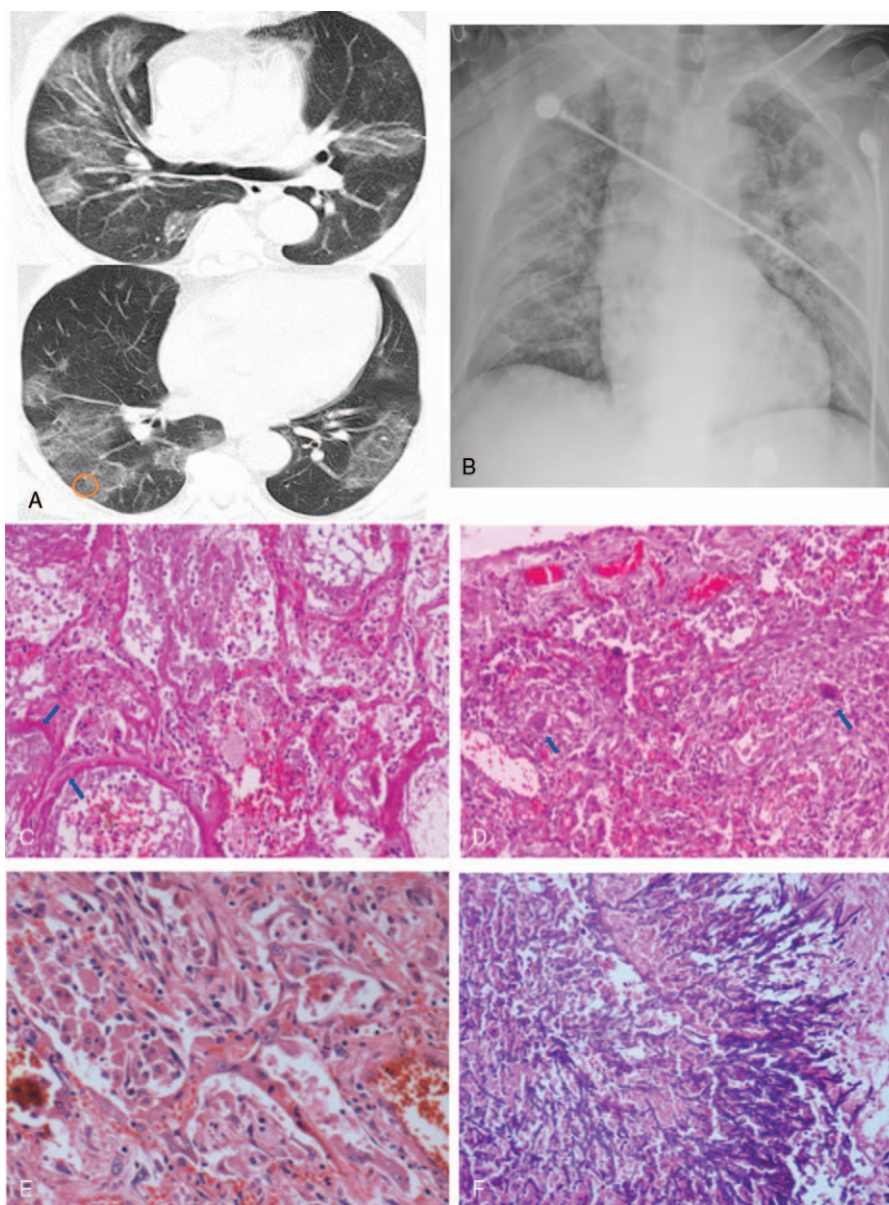


Figure 3. A: At the 15th day, a large degree of patchy ground-glass opacities along the bronchus and periphery with superposed vasodilation, interstitial thickening were observed. B: “white lungs,” manifested as obvious ground-glass opacities and fibrosis (the 21st day from onset). C: In the central part of the right lower lobe, fibrin exudate, hyaline membrane formation (arrows) and inflammatory cell infiltration in alveoli. Hyperemia and thickening of the alveolar wall, part of which was replaced by fibrous tissue ($\times 100$). D: In the subpleural part of the right lower lobe, alveolar structure destruction was seen. The granuloma nodules were composed of epithelioid cells and multinucleated giant cells (arrows) with central suppuration ($\times 40$). E: Fibroblast proliferation and a large number of monocyte and lymphocytes infiltration. ($\times 200$) F: Secondary fungal infections with *Aspergillus* mycelium in the subpleural part of right lower lobe ($\times 100$). Yellow circle: subpleural pathological sampling site.

of bronchioles and terminal bronchioles, and type II pneumocytes. SARS-CoV-2 can invade into the epithelium by binding to the ACE2 receptor,^[11] which may underlie why the majority of lesions are first identified in subpleural areas. This is consistent with the attack pattern of viral pneumonia.^[12] Then capillaries contractions and reduced blood-oxygen exchange are induced, causing pneumoedema^[13] and exudation. These early pathological changes can be captured by high-resolution CT.

More obvious fibrosis and alveolar structure destruction in subpleural areas were supported by radiological and pathological examinations. Radiological and gross examinations revealed that lesions in the margin areas were more severe. Our histological

findings showed some differences between central and subpleural areas. At the periphery, fibrous tissue proliferation in the alveolar septa and alveolar destruction were remarkably abundant. However, in the central area, the alveolar structure was roughly preserved with only focal fibrosis within alveolar septa. Serous and macrophages exudation were apparent within the alveolar space. This may be related to the temporal and spatial changes and the severity of lesions. The lesions in the periphery generally appeared earlier and lasted longer and thus were more severe than those in the center of the lobe. This was also consistent with CT manifestations showing that GGO and fibrosis usually began in subpleural areas. As the disease progressed, more opacities of a larger size and higher

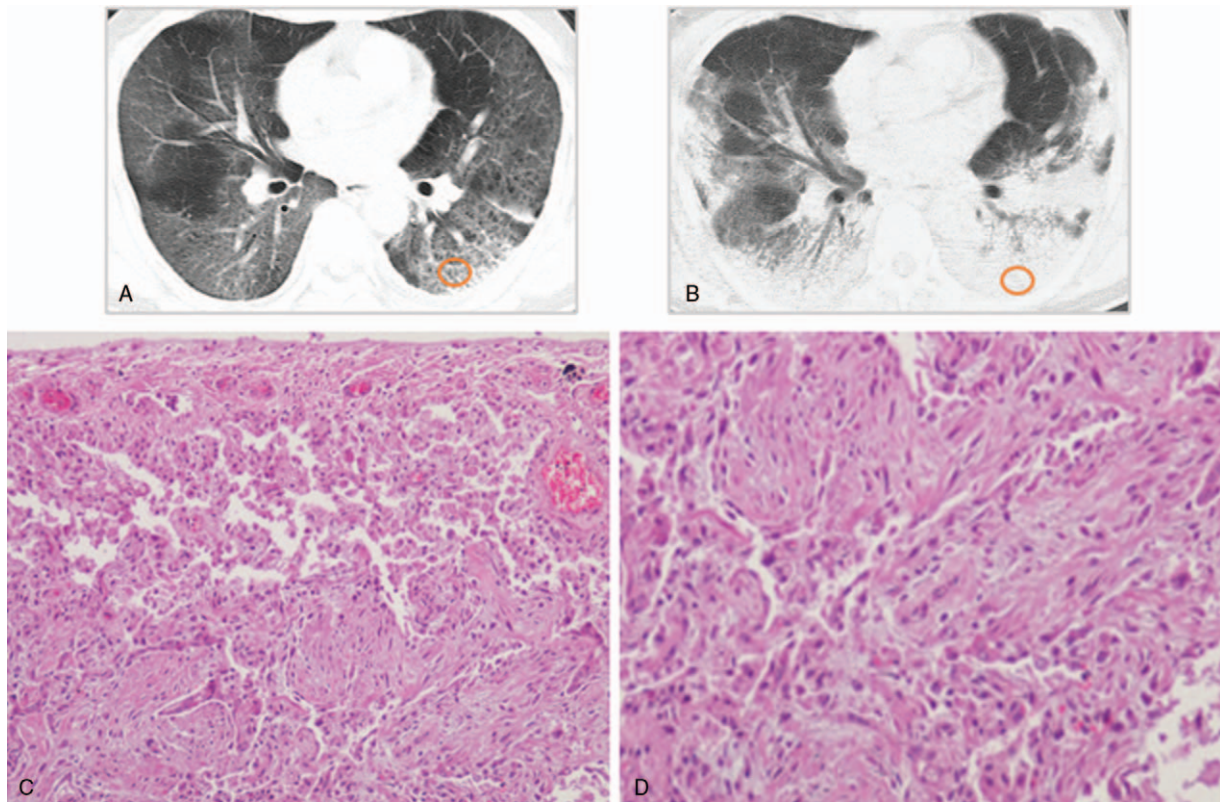


Figure 4. A: A large degree of patchy ground-glass opacities with interstitial thickening or reticulation. “paving stone signs” were seen (17th day after onset). B: 7 days later, larger scale and higher density of the lesions, and pleural thickening indicated a progression. Consolidation, fibrosis, bronchiectasis, bronchial traction and small air-sacs were presented, particularly in the periphery. C: Pulmonary fibrosis and alveolar destruction in the subpleural part of the dorsal side of the left upper lobe ($\times 100$). D: Fibrous tissue proliferation in the alveolar septa, alveolar collapse, organized exudate in alveoli, alveolar epithelium exfoliation and adenoid alveolar formation ($\times 200$). Yellow circle: subpleural pathological sampling site.

density were seen, including the central areas of the lung. Most cases in this cohort had this characteristic (for e.g., 2, 3, and 4).

In addition to the characteristic distribution manner, diverse GGOs are the fundamental imaging sign of COVID-19 pneumonia.^[8–10] The pathogens invade the bronchioles and alveolar epithelium and replicate, causing exudation, which was composed of the involved epithelium, lymphocytes and other inflammatory cells, protein and fibrin, forming a membranous substance in the alveolar space. This hampers blood-oxygen exchange and causes subsequent dyspnea.^[14] GGO with consolidation and/or interlobular septal thickening, sometimes manifested as “paving stone signs,” were also the main CT features, as well as “white lungs”,^[8–10] which was the worst outcome. The pathological findings manifested as fibrous tissue proliferation in the alveolar septa and interlobular septa. Fibroblast proliferation, type II alveolar epithelium hyperplasia, adenoid alveolar formation and filled alveoli with organizing exudation then lead to consolidation.

In our study, hyaline membranes were common seen in critically ill and end-stage cases. In another study, 2 patients who underwent lung lobectomies for cancer were retrospectively found to have COVID-19 at the time of surgery. In the asymptomatic and early phase, hyaline membranes were not prominent.^[15] As a result, if serious GGOs or even obvious consolidation and interlobular septal thickening, which is fundamentally based on extensive exudation, hyaline membrane formation and fibrosis, were observed shortly after symptom

onset, it usually indicates a potential risk of adverse CT and clinical outcomes over short-term follow-up. Radiological examinations, especially high-resolution CT, are of considerable value for the early identification of individuals who are at risk of becoming critically ill and who will most likely benefit from intensive care treatment. However, it remains challenging to distinguish fibrosis-based or organizing exudation-based consolidation from CT images.

These features of SARS-CoV-2 infection bear some resemblance to those of some other beta-coronavirus infections, for example the highly homologous SARS-CoV.^[16,17] In SARS, patients with longer illness duration also exhibited more fibrosis than those of patients with shorter illness duration.^[16] Lesions with longer courses exhibited more evident fibrosis was one of the similarities. However, this fibrosis, manifested as fibroblasts proliferation and type II alveolar epithelium hyperplasia, may occur earlier in COVID-19. In SARS, the fibrosis was not evident in 3 cases over 10 to 20 days of disease duration,^[18] as well as another case with a 14 day duration.^[14] Extensive fibrosis was observed in later stages.^[16] However, in the current study on COVID-19 the fibrosis was obvious in all 9 cases, including 3 cases with disease durations of 14, 18, and 20 days.

Furthermore, while persistent infection by SARS-CoV-2 may result in on-going pulmonary vascular-endothelial injury, coexistent superinfections (for example the *Aspergillus* and *Acinetobacter baumannii* infections in case 3 and case 5) may also contribute significantly to morbidity and mortality in some

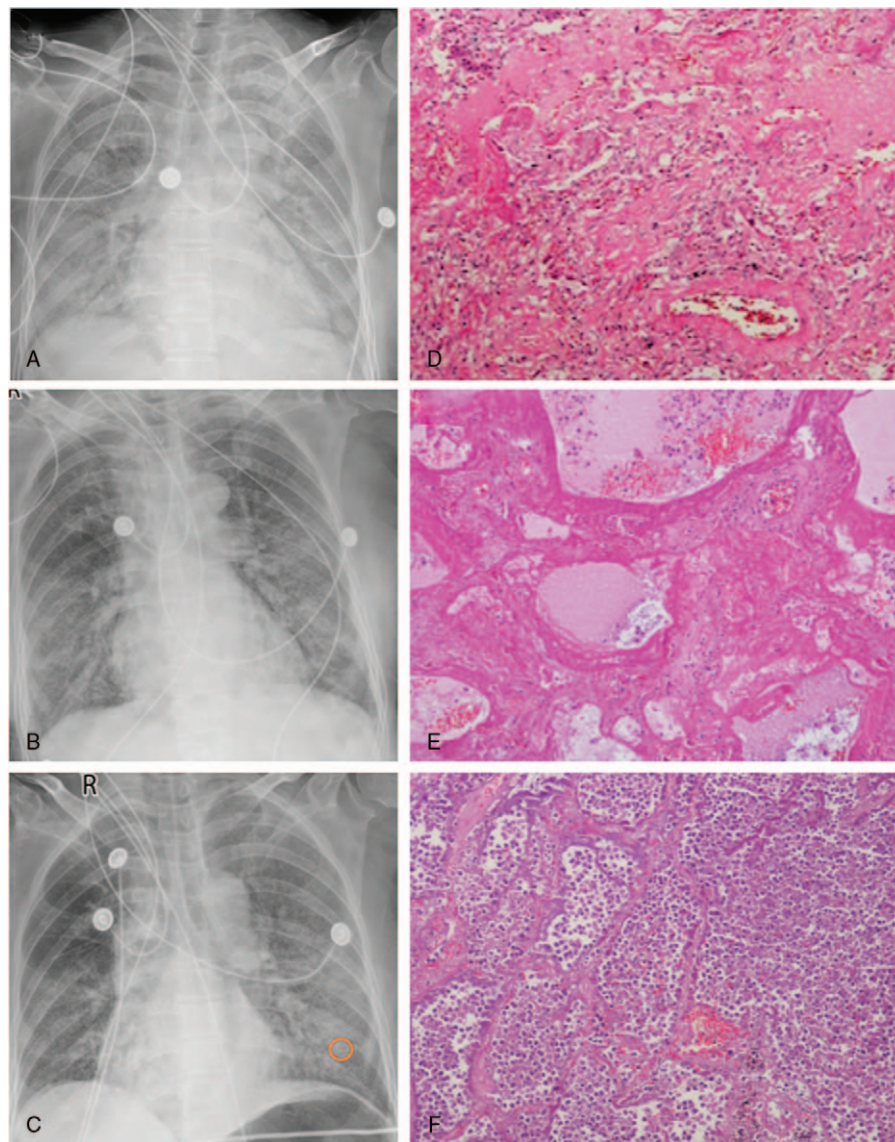


Figure 5. A: “White lungs” (23rd day after onset). B: The increased transparency of bilateral lungs indicated an improvement (26th day after onset). C: A large degree of patchy ground-glass opacities with interstitial thickening or reticulation were observed in the left upper and lower lobes (28th day from onset). CR image showed bronchopneumonia in the left lower lobe. D: Alveolar structure destruction, widened alveolar septum and focal hemorrhagic necrosis. Diffuse alveolar damage with hyaline membrane formation and alveolar septal fibrosis, pulmonary congestion and edema in the left lower lobe ($\times 40$). E: Hyaline membrane and alveolar exudation in the left lower lobe ($\times 100$). F: Secondary bacterial infection in the left lower lobe: a large number of neutrophil exudations in the alveolar spaces (suppurative inflammation). The alveoli structures were still preserved ($\times 100$). Yellow circle: pathological sampling site for suppurative infection.

patients. High-resolution CT may be helpful in identifying pure viral pneumonia and secondary bacterial pneumonia. The value of bedside CR films, however, is limited compared to CT. The sudden reappearance of enlarged patchy GGO, combined with a clinical condition change and laboratory tests, allowed clinicians to raise the possibility of bacterial coinfection in case 5. Our pathology found that 6 of the 9 cases exhibited co-infection with bacterial or fungal infections. Thus, nosocomial infection and secondary infections should be taken seriously, especially during mechanical ventilation.

This study has some limitations. First, only 9 cases, those with complete history, radiological and pathological data, were included. It was often quite difficult to persuade the families of each case to agree to an autopsy. Second, compared with lung

biopsies, there may have been some deviations between pathological sampling sites and the corresponding locations of images. Third, because of the rapid progression of this disease, in the critically ill stage, the last radiographic data available in this study and the data closest to the time of pathological examination was usually obtained via bedside CR films and therefore lacked sufficiently detailed imaging evidence, which high-resolution CT may supply.

This study revealed the pathogenesis of the pulmonary damage of COVID-19, and further indicates the relationship between diverse pulmonary opacities, consolidation and other alterations in radiological images and histopathological findings. The CT and clinical characteristics, such as ground-glass opacities with consolidation, subpleural area originated and preference, early-stage fibrosis and a propensity to be infected with other

Table 2**Summary of the final laboratory examinations of the COVID-19 patients.**

Index	Values; Median (IQR)	Normal range
White blood cell count $\times 10^9/L$	14.9 (13.1–17.1)	3.5–9.5
Neutrophil count $\times 10^9/L$	14.6 (12.2–17.0)	1.8–6.3
Lymphocyte count $\times 10^9/L$	0.73 (0.62–0.84)	1.1–3.2
Red blood cell count $\times 10^{12}/L$	4.0 (3.8–4.2)	3.8–5.5
Hemoglobin, g/L	119.0 (113.0–127.5)	130–175
Platelet count $\times 10^9/L$	167.0 (116.5–169.5)	125–350
Alanine aminotransferase ALT, U/L	107.5 (78.2–158.7)	≤ 41
Creatinine, $\mu\text{mol}/L$	194.4 (93.2–339.8)	59–104
Lactate dehydrogenase, U/L	583.0 (502.5–589.0)	135–225
Hypersensitive cardiac troponin I, pg/ml	206.6 (110.3–962.7)	≤ 15.6
B-type natriuretic peptide, pg/mL	156.8 (120.3–567.8)	< 285
D-dimer, $\mu\text{g}/\text{ml}$	16.6 (12.5–34.3)	< 0.5
Procalcitonin, ng/ml	0.12 (0.12–0.12)	0.02–0.05
C-reactive protein, mg/L	160.0 (152.7–160.0)	< 10
Ferritin, $\mu\text{g}/L$	1600 (1550–1800)	30–400
Erythrocyte sedimentation rate, mm/h	75.0 (59.5–82.0)	0–15
Interleukin 6, pg/ml	10.8 (10.7–17.8)	< 7
eGFR, ml/min/1.73m ²	26.7 (10.9–68.9)	80–120

IQR = interquartile range.

Table 3**Summary of histologic features in lungs of the COVID-19 patients.**

Histological features	Numbers of cases
Acute fibrinous exudate	9
Fibrosis	9
Hyaline membranes	9
Pulmonary edema	9
Hemorrhage	9
Pneumocyte hyperplasia	9
Thromboemboli	7
Secondary infections (bacterial or fungal infection)	6

pathogens, were thus correlated with evidence from histopathological examinations.

Acknowledgment

We express our highest respect to the donor patients, and thank the patients and their families for their willingness to provide consent for postmortem and pathological examinations; all histotechnologists for their assistance in histopathological sample preparation.

Author contributions

Data curation: Yanqing Fan.

Investigation: Lingyun Zhao, Xi Wang, Ying Xiong, Yiwu Zhou.

Methodology: Lingyun Zhao, Xi Wang, Ying Xiong, Yiwu Zhou.

Project administration: Wenzhen Zhu.

Resources: Xi Wang, Ying Xiong, Yanqing Fan, Yiwu Zhou, Wenzhen Zhu.

Validation: Lingyun Zhao, Wenzhen Zhu.

Visualization: Xi Wang, Yanqing Fan.

Writing – original draft: Lingyun Zhao, Ying Xiong.

Writing – review & editing: Xi Wang, Wenzhen Zhu.

References

- [1] International Committee on Taxonomy of Viruses. Naming the 2019 Coronavirus. Available at: <https://talk.ictvonline.org/>. [accessed February 11, 2020]
- [2] Zhu N, Zhang D, Wang W, et al. A novel coronavirus from patients with pneumonia in China, 2019. *N Engl J Med* 2020;382:727–33.
- [3] World Health Organization. Weekly epidemiological update - December 29, 2020. Available at: <https://www.who.int/publications/m/item/weekly-epidemiological-update-29-december-2020>
- [4] Huang C, Wang Y, Li X, et al. Clinical features of patients infected with 2019 novel coronavirus in Wuhan, China. *Lancet* 2020;395:497–506.
- [5] Chen N, Zhou M, Dong X, et al. Epidemiological and clinical characteristics of 99 cases of 2019 novel coronavirus pneumonia in Wuhan, China: a descriptive study. *Lancet* 2020;395:507–13.
- [6] Wang D, Hu B, Hu C, et al. Clinical characteristics of 138 hospitalized patients with 2019 novel coronavirus-infected pneumonia in Wuhan, China. *JAMA* 2020;323:1061–9.
- [7] Yang X, Yu Y, Xu J, et al. Clinical course and outcomes of critically ill patients with SARS-CoV-2 pneumonia in Wuhan, China: a single-centered, retrospective, observational study. *Lancet Respir Med* 2020;8:475–81.
- [8] Shi H, Han X, Jiang N, et al. Radiological findings from 81 patients with COVID-19 pneumonia in Wuhan, China: a descriptive study. *Lancet Infect Dis* 2020;20:425–34.
- [9] Chung M, Bernheim A, Mei X, et al. CT imaging features of 2019 novel coronavirus (2019-nCoV). *Radiology* 2020;295:202–7.
- [10] Xiong Y, Sun D, Liu Y, et al. Clinical and high-resolution CT features of the COVID-19 infection: comparison of the initial and follow-up changes. *Invest Radiol* 2020;55:332–9.
- [11] Lu R, Zhao X, Li J, et al. Genomic characterisation and epidemiology of 2019 novel coronavirus: implications for virus origins and receptor binding. *Lancet* 2020;395:565–74.
- [12] Koo HJ, Lim S, Choe J, et al. Radiographic and CT features of viral pneumonia. *Radiographics* 2018;38:719–39.
- [13] Imai Y, Kuba K, Rao S, et al. Angiotensin-converting enzyme 2 protects from severe acute lung failure. *Nature* 2005;436:112–6.
- [14] Xu Z, Shi L, Wang Y, et al. Pathological findings of COVID-19 associated with acute respiratory distress syndrome. *Lancet Respir Med* 2020;8:420–2.
- [15] Tian S, Hu W, Niu L, et al. Pulmonary pathology of early phase 2019 novel coronavirus (COVID-19) pneumonia in two patients with lung cancer. *J Thorac Oncol* 2020;15:700–4.
- [16] Hwang DM, Chamberlain DW, Poutanen SM, et al. Pulmonary pathology of severe acute respiratory syndrome in Toronto. *Mod Pathol* 2005;18:1–0.
- [17] Franks TJ, Chong PY, Chui P, et al. Lung pathology of severe acute respiratory syndrome (SARS): a study of 8 autopsy cases from Singapore. *Hum Pathol* 2003;34:743–8.
- [18] Ding Y, Wang H, Shen H, et al. The clinical pathology of severe acute respiratory syndrome (SARS): a report from China. *J Pathol* 2003;200:282–9.